MATERIALS SCIENCE

Stimulated transformation of soft helix among helicoidal, heliconical, and their inverse helices

Cong-long Yuan[1]*, Wenbin Huang[1,2]*, Zhi-gang Zheng[1,3,4]*†, Binghui Liu[1], Hari Krishna Bisoyi[5], Yannian Li[5], Dong Shen[1], Yanqing Lu[3]†, Quan Li[5]†

Dynamic modulation of soft helix in terms of the molecular organization, handedness, and pitch length could result in a sophisticated control over its functions, opening numerous possibilities toward the exploration of previously unidentified applications. Here, we report a dynamic and reversible transformation of a soft helical superstructure among the helicoidal (molecules orthogonal to helical axis), heliconical (molecules oblique to the helical axis, i.e., oblique helicoidal), and their inverse helices, together with a tunability on the helical pitch, by combining electrical and optical manipulations. This multistate transformation depends on a matching of the temperature, the strength of external stimuli, and the bend and twist elastic effects of the system. A laser emission with tunable wavelength and polarization, and prescribed micropatterns formed by any aforementioned architectures were achieved.

INTRODUCTION

Hierarchically organized helical or spiral structures are omnipresent in nature, e.g., twisted plywood collagen patterns in bones (*1*), nested arc microstructures in beetle cells (*2*), and cellulose-based periodically twisted stacks on fruit peels (*3*, *4*). The control of helicity is of fundamental importance, as it allows an easy transformation among different enantiomers with disparate chemical, physical, and biological functions. For instance, the helicity of the superstructure formed from asymmetric dumbbell magnetic colloids can be controlled by the sphere ratio (*5*); spiral superstructure arrays of magnetic cubic nanocrystals self-assembled at the liquid-air interface could be switched among single, double, and triple helices by varying the nanocrystal densities (*6*); achiral spherical colloids could assemble into helical chains in the V-groove, and the handedness is controlled by the capillary force direction (*7*); and chiral colloidal phage could produce multiple-level helical conformations including nematic orthogonal twists, cholesteric helical ribbons, and smectic helicolidal nanofilaments, depending on the phage concentration and the pulling speed (*8*). In addition, molecular self-organization behaviors of a helical superstructure and its corresponding chiroptical capabilities under the influence of an external stimulation have been under intense investigation for realizing novel active or tunable devices with dynamic characteristics. The double helix formed by two strands of DNA can be flipped from the right-handedness helix to the left-handedness conformation under suitable salt and temperature environment, thereby producing a rotary or linear motion as nanomachines (*9*, *10*). The supramolecular helix of naphthalenediimide chromophores shows opposite handedness on binding with different adenosine phosphates, allowing a real-time monitoring into the adenosine triphosphate hydrolysis kinetics (*11*). Materials that could show reliable, dynamic, and reversible helix transformation with controllable hierarchical complexities are in demand as they are of substantial importance in terms of their self-organization kinetics and novel applications.

The liquid crystalline phase could self-organize into stable or transient superstructures with helical features (i.e., cholesteric phase) induced by intermolecular interactions and external stimuli. In the cholesteric phase, liquid crystal (LC) molecules rotate around the helical axis, and the molecular long axes are perpendicular to the helical axis, i.e., the common helical superstructure exists in the majority of the cholesteric LC. Sustaining efforts have been devoted in the last decade to dynamically manipulate the physical parameters of these helicoidal superstructures, such as the helical pitch length, helical handedness, and even the direction of the helical axis, by electric field, light, and heat, thereby exhibiting diverse performances and applications in photonics (*12*–*15*). In the case that cell substrates are treated with an alignment layer with a precisely controlled pretilt angle, the LC molecular director shows a symmetrically gradient twist angle from the cell surface to the middle layer; however, it shows no periodic spiral texture (*16*). Moreover, chiral smectic C phase exhibits a helix with a certain invariable molecular tilt angle arranged in layered architectures, giving rise to its ferroelectric properties (*17*) with binary switching states in terms of the tilt cone. Recently, a specific nematic phase designated as the twist-bend nematic (N_{tb}) phase has been characterized in various bent-shaped LC dimeric compounds, in which the molecules rotate around the helical axis, but with an oblique angle to the axis rather than perpendicular as aforementioned helicoidal structure (*18*–*20*), i.e., heliconical helix, showing reversible N_{tb} phase transition upon photoisomerization of the azo linkage in the LC dimer (*21*). This structure with a short pitch of about 10 nm is energy degenerated, allowing the coexistence of both right-handedness and left-handedness twists, and thus, it consists of inhomogeneously distributed domains in uncontrollable handednesses. The ability to switch among helicoidal and heliconical helices and their counterparts with inverse handedness with controlled parameters in a single material system remains elusive and has not been achieved in soft matters to the best of our knowledge. Here, we propose a stimuli-activated helical cholesteric soft superstructure, presenting reversible and dynamic transformations between helicoidal and heliconical

[1]Department of Physics, East China University of Science and Technology, Shanghai 200237, China. [2]School of Optoelectronic Science and Engineering and Collaborative Innovation Center of Suzhou Nano Science and Technology, Soochow University, Suzhou 215006, China. [3]National Laboratory of Solid State Microstructures, Collaborative Innovation Center of Advanced Microstructures and College of Engineering and Applied Sciences, Nanjing University, Nanjing 210093, China. [4]State Key Laboratory of Applied Optics, Changchun Institute of Optics, Fine Mechanics and Physics, Chinese Academy of Sciences, Changchun 130033, China. [5]Advanced Materials and Liquid Crystal Institute and Chemical Physics Interdisciplinary Program, Kent State University, Kent, OH 44242, USA.
*These authors contributed equally to this work.
†Corresponding author. Email: zgzheng@ecust.edu.cn (Z.-g.Z.); yqlu@nju.edu.cn (Y.Lu); qli1@kent.edu (Q.L.)

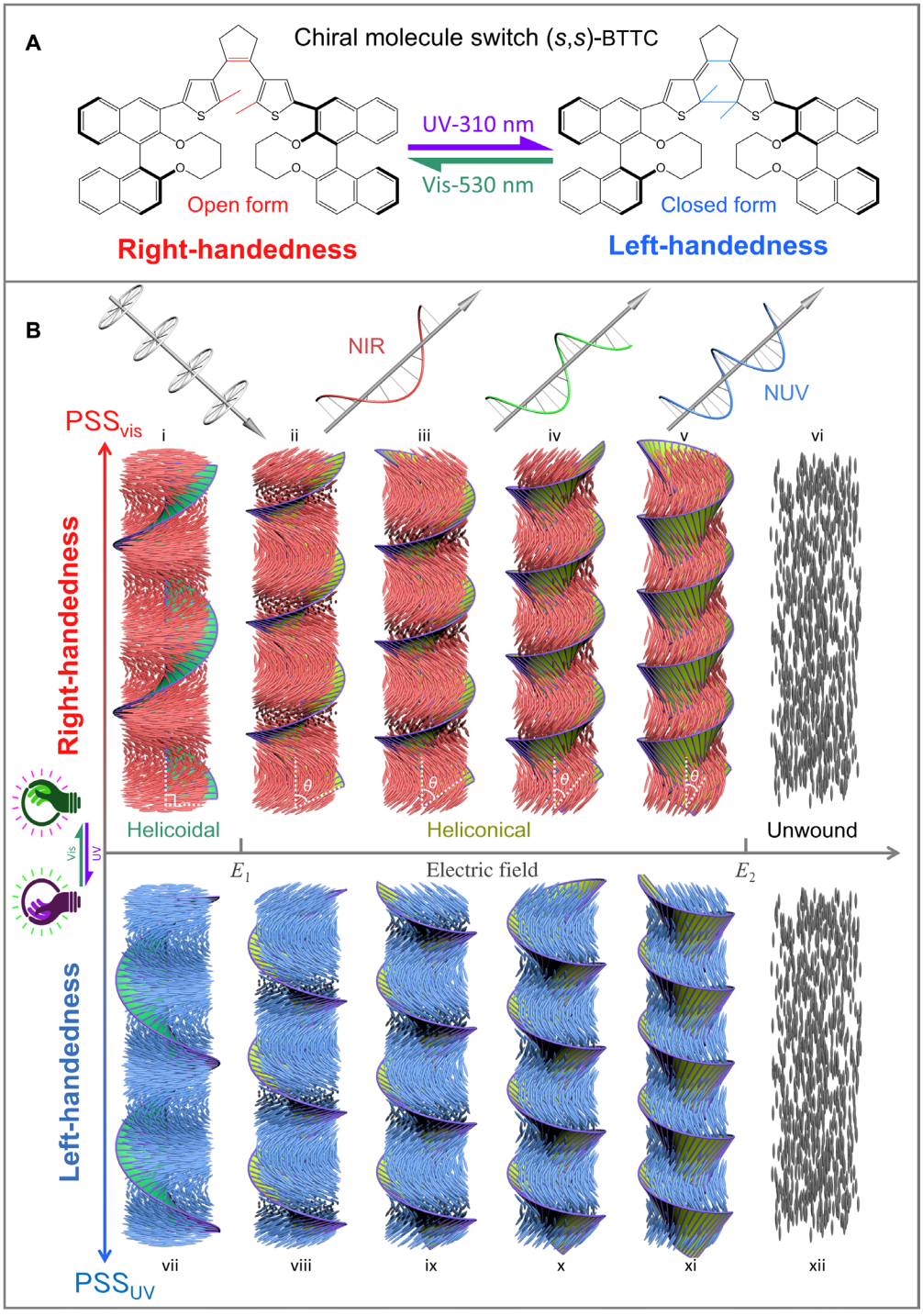

Fig. 1. Helix transformation based on a photoresponsive cholesteric LC system by dual stimulation with electric field and light. (**A**) Molecular structures of the photodynamic chiral molecular switch (*s*,*s*)-BTTC in the ring-open form and the ring-closed form, acting as the chiral motor for the right-handedness and left-handedness helices, respectively. The ring-open structure transforms into the ring-closed isomer and backward upon irradiation with UV (310 nm) and visible (530 nm) light, respectively. Both isomers are fatigue resistant with no thermal relaxation. (**B**) Schematic illustration of the transformations among the diverse LC helices under the dual stimulation of electric field and light. The top and bottom panels of helical superstructures are in the PSS_{vis} and PSS_{uv} states, respectively. The electric field across the LC cell is the driving force for the transition among different helical superstructures in the same handedness, while suitable light irradiation imposes a reversible handedness inversion between the two panels. (i) The right-handedness and (xii) the left-handedness helicoidal superstructures with the LC director being perpendicular to the helical axis, $E < E_1$. (ii) The right-handedness and (vii) left-handedness heliconical superstructures, in which the LC director is tilted with an oblique angle of θ to the helical axis, $E > E_1$. The heliconical pitch length *P* and oblique angle θ decrease as the electric field increases, resulting in a wide spectral range tunability of the reflection spectrum from the NIR to the NUV band for the right-handedness (ii to v) and left-handedness (viii to xi) heliconical superstructures, respectively. (vi and xii) The unwound homeotropic nematic state, $E > E_2$. Here, E_1 and E_2 are the thresholds of the transition from the helicoidal helix to the heliconical helix and the unwinding electric field of a heliconical helix, respectively.

states accompanied with a handedness inversion and a modulation of helical pitch length and the oblique angle of the heliconical states under the influence of a dual stimulation of electric field and light. This work could facilitate better understanding of some mystical but inevitable natural phenomenon, for instance, the opposite handedness of the horn of *Tragelaphus strepsiceros* and the heliconical architecture of *fusilli paesani*, and thereby could build a bridge between soft condensed matter physics and biology and linking the macroscopic geometric structures to the microscopic molecular self-organization.

RESULTS AND DISCUSSION

We have judiciously designed a material system, enabling a photoresponsive helical structure, showing a reversible and dynamic transformation among helicoidal state, heliconical state, and their corresponding handedness inverted helices under a cooperated stimulus of electric field and light. The material system is mainly composed of an achiral LC dimer denoted as CB7CB (fig. S6), the commercial nematic LC E7, and an efficient photosensitive dithienylcyclopentene-based axially chiral molecular switch, denoted as (*s*,*s*)-BTTC (Fig. 1A). The CB7CB, with two cyanobiphenyl mesogens connected by a flexible chain with an odd number of carbons, furnishes necessary bend and twist elastic effects to induce and stabilize the heliconical superstructure in the cholesteric phase. The concentration of the nematic LC E7 was delicately optimized to enable room temperature cholesteric phase of the material system (fig. S7). The chiral molecular switch used here undergoes reversible isomerization between its ring-open and ring-closed isomers with suitable light irradiation. Upon irradiation with ultraviolet (UV) light at (310 nm, 1.8 mW/cm^2) for about 300 s, the ring-open isomer is transformed into the ring-closed isomer. The reverse process occurs upon irradiation with a visible light (530 nm, 5.5 mW/cm^2) for about 400 s. The helical twisting power (HTP) of the molecular switch in the host mixture containing E7 and CB7CB determined in a wedge cell was +8.0 and −16.0 μm^{-1} in the ring-open and ring-closed states, respectively. The positive HTP value indicated the right-handedness of the LC helix induced by the ring-open isomer, while the minus sign denotes the opposite handedness caused by the ring-closed isomer, thus achieving reversible handedness inversion. Furthermore, it is noteworthy that the photoresponsive chiral molecular switch shows excellent fatigue resistance with superior thermal stability (*22*), i.e., almost no thermal relaxation (fig. S8), in both ring-open and ring-closed states when compared with the common azobenzene-based materials, facilitating stable dynamic operation. A small amount [0.5 weight % (wt %)] of photoinsensitive commercial right-handed chiral agent R811 was mixed to achieve comparable initial pitch of the cholesteric LC (CLC) system in the PSS_{vis} and PSS_{UV} states, thereby ensuring a similar dynamic spectral range of reflection band with regard to the right- and left-handed heliconical structures. The mixture was then injected into a 35-μm-thick LC cell with planar alignment for the subsequent investigations.

Figure 1B schematically demonstrates the reversible manipulation among diverse LC helices by a cooperated stimulation of electric field and light. The upper panel indicates helix transformation stimulated by the electric field at the photostationary state (PSS) after the sample is irradiated by visible light, i.e., PSS_{vis} state, while the lower part depicts the transformation at an opposite PSS induced by UV light exposure, i.e., PSS_{UV} state. Initially, LC molecules arranged to a right-handedness helicoidal helix (Fig. 1B, i) with an initial pitch length P_0 around 2.6 μm determined by the HTP and the concentration of the chiral agents. An electric field applied across the LC cell triggered an arrangement transformation from helicoidal to heliconical (Fig. 1B, ii) helix when the strength was over a threshold, denoted as E_1, due to the coupling and competition effects of the dielectric torque and the twist torque (fig. S1 and eq. S7). A continuous enhancement of the electric field led to a gradual tilt of LC molecules, i.e., the decrease in the oblique angle, and accompanied by a reduction in the helical pitch length, which caused a blueshift of the corresponding selective reflective wavelength [Fig. 1B (ii to v), fig. S3, and eqs. S8 and S9]. The field-induced heliconical state was not infinitely compressed but unwound and transited to a homeotropic alignment (Fig. 1B, vi) as the electric field was further enhanced to the unwinding strength of E_2 as denoted (eq. S6). As predicted, a recovery was achieved just by reducing the electric field gradually. We have theoretically shown that tuning ranges of the relative pitch P/P_0 and the oblique angle θ depend solely on the ratio between the bend and the twist elastic constants of the material system, irrespective of the chirality (fig. S2). Note that each heliconical arrangement was stable (i.e., the pitch length and oblique angle are constant) as long as the electric field was maintained. Each right-handedness helix, whatever helicoidal or heliconical state, can be modulated to a corresponding arrangement but with an opposite helical handedness by a UV exposure to stimulate the sample to the PSS_{UV} state, caused by the effect of the chiral molecular switch (*s*,*s*)-BTTC. However, the electric field should be applied to keep the oblique orientation of LC molecules in the heliconical state. The reversible tuning among the left-handedness helices can be realized by the electric field as the same (Fig. 1B, vii to xii), while the transformation between two opposite handedness helices can be controlled reversibly by alternate irradiation with UV and visible light. As aforementioned, the intermediate state with left-handedness is still stable due to the excellent fatigue resistance of (*s*,*s*)-BTTC. Therefore, any helical soft superstructure, including helicoidal, heliconical helix, and their inversed counterpart, can be accurately directed under a coordinated influence of electric field and light stimulations.

The aforementioned modulation was demonstrated further through optical textures and spectroscopy. A right-handedness helicoidal helix showing a focal conic texture was observed when the electric field was absent (Fig. 2A, i), which was slightly different with that of common cholesteric LC confined by the same boundary condition, due to the specific bent molecular geometry of the LC dimer in the mixture. When the electric field exceeded the transformation threshold between helicoidal and heliconical arrangements and reached 0.67 V/μm, the texture presented a uniform dark state (Fig. 2A, ii), indicating the heliconical structure. It was further analyzed theoretically (sections S1 and S2) and confirmed from the tested reflection spectrum (Fig. 2B) and the simulated reflection behavior based on Berreman's 4 × 4 matrix method (fig. S3) (*23*), which indicated a conspicuous reflection peak at the near-infrared (NIR) band caused by the selective reflection characteristic of the heliconical structure rather than the scattered focal conic state of the helicoidal one. Further increase in the electric field resulted in a compression of the pitch length verified from the successive change of reflection color to a visible bright red, orange, bright green, dark cyan, and dark blue (Fig. 2A, iii to vii), corresponding to a blueshift of the spectra (Fig. 2B). The reduction in reflection bandwidth and reflectance as the enhancement of electric field related to the shortening of the pitch length and the decrease in the oblique angle. It is worth mentioning here that these reflection spectra can be reversibly modulated by the electric field in a rather wide spectral range from the NIR, spanning across the entire

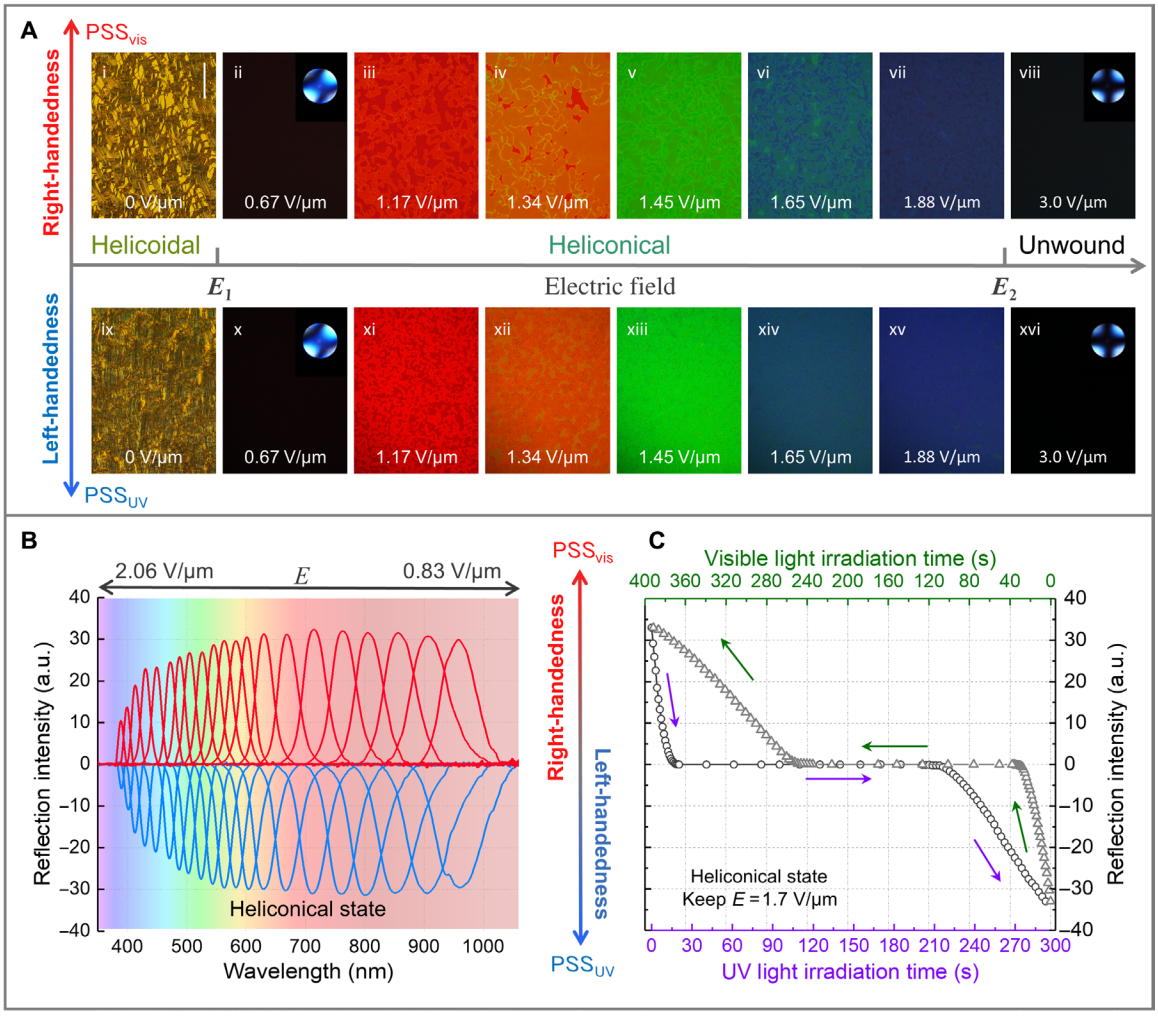

Fig. 2. Performance of soft superstructure transformation with electrical and optical stimuli as driving parameters. (**A**) Texture images of different helical superstructures under the polarizing optical microscope, which indicate the helicoidal superstructure at 0 V/μm, the heliconical superstructures with varying pitches from 0.67 to 1.88 V/μm, and the unwound state at 3.0 V/μm. Some dislocation lines can be observed due to the nucleation process during the pitch adjustment. Scale bar, 300 μm. The insets of (ii), (viii), (x), and (xvi) are the conoscopic images at the corresponding states. (**B**) Measured reflection spectra from the heliconical superstructures in the NUV, visible, and NIR range. The electric field is the stimulus to drive the helix transformation in the PSS_{vis} state or the PSS_{uv} state for the right-handedness or the left-handedness helix, respectively. On the other hand, UV and visible light irradiation drives the helix transformation downward and upward between the two panels, inverting the handedness. The positive and negative intensity value denotes the reflection from the right-handedness and left-handedness heliconical superstructures, respectively. a.u., arbitrary units. (**C**) Handedness switching performance of the helical superstructure using light stimulus. Reflection intensity and handedness as a function of the irradiation time using the UV (circles) and visible light (triangles) on the initial PSS right-handedness and left-handedness heliconical superstructures, respectively. The applied electric field was maintained as 1.17 V/μm throughout the whole optical tuning process. The reflection central wavelength merely changes during the switching process. A light source at the central wavelength of 310 nm (1.8 mW/cm^2) and 530 nm (5.5 mW/cm^2) was used for UV and visible irradiation, respectively.

visible band, to the near-UV (NUV) band (Fig. 2B); however, the corresponding texture reflecting the NUV band was not shown here, limited by the capability of the polarized optical microscope (POM). This performance was probably dependent on a delicate equilibrium between bend and twist elastic effects and a competitive coupling of the twist and dielectric torques of the system, which was quite different with the electric field–induced layer undulation of the common cholesteric LC, generally presenting fingerprint texture, or the flexoelectric effect caused by the dipole interaction of an asymmetric molecular distribution, or even the molecular dipole effect in the ferroelectric LC (*24*–*26*). Furthermore, temperature also plays a nonneglected role on both the helix transformation and the reflection spectrum modulation (fig. S7), probably resulting from the change of equilibrium between the bend and twist elastic effects. As the electric field was strong enough, e.g., 3.0 V/μm, the heliconical structure cannot be maintained and unwound to the field-induced optically isotropic homeotropic alignment state, which was further confirmed by the Maltese cross observed with a conoscope (Fig. 2A, viii and inset) since the dielectric torque in this case overwhelmed the twisted torque. The handedness inversion of the system was implemented by an irradiation of 310-nm UV as aforementioned. The blueshift of reflection band for the opposite handed heliconical structure, covering almost the same spectral range from NIR to NUV (Fig. 2B and fig. S5) and exhibiting the corresponding change of the reflection color from red, green to blue (Fig. 2A, ix to xvi), was observed. These performances indicate that the delicate elastic equilibrium of the system

does not depend on the photoisomerization of (*s*,*s*)-BTTC. The handedness here was detected by testing the polarization state of reflected light under the illumination of a white light source (see Materials and Methods and section S6). The handedness inversion process could be corroborated by a decrease followed by an increase in the reflection intensity obtained by the integral area of the spectral reflection band of the sample (i.e., E = 1.17 V/μm; Fig. 2A, iii) in the process of UV and visible light irradiation, respectively (Fig. 2C). In addition, the reflection band showed a small blueshift of less than 10 nm and accompanied by a decrease in reflection intensity in this case, which was further confirmed by theoretical simulation (figs. S4 and S5). Notably, a coupling among the light, electric field, and twist and bend elastic effects enabled the whole arrangement transformation of the self-organized helical superstructure. A modulation of irradiation energy inevitably broke this coupling and the original elastic equilibrium of the system, giving rise to the prominent changes on both the arrangement transformation of the helix and the performance of reflection spectrum modulation. It means that the heliconical superstructure in the system can be reversibly switched between existence and disappearance; in addition, the capability of modulating the spectral reflection can be readily controlled by light as well (figs. S4 and S5). Therefore, an accurate helix manipulation with a digital point-by-point or line-by-line matrix scanning was achieved, which might be a great potential technique in not only the photonics but also the soft material configurations and even the biotherapy.

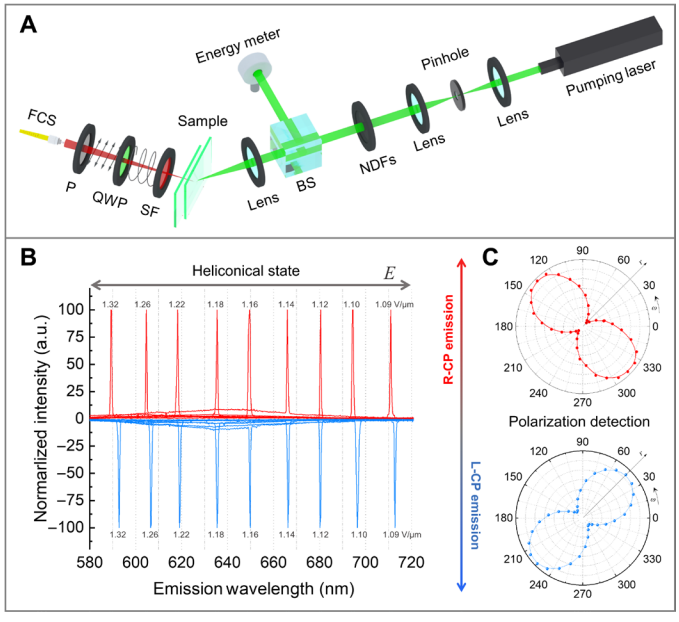

Fig. 3. Wavelength and polarization tunable mirrorless lasing from the heliconical superstructure. (**A**) Illustration of the experimental setup for the characterization of laser performance (see Materials and Methods). NDFs, neutral density filters; BS, beam splitter. Output emission to the sample normal was analyzed using a fiber-coupled spectrometer (FCS) by rotating the polarizer (P), where the residue pump beam was blocked by a spectral filter (SF; cutoff wavelength, <550 nm). A quarter wave plate (QWP) at the wavelength of 632 nm was used to convert the circularly polarized emission into linear polarization. (**B**) Laser emission spectra from the heliconical superstructures with right-handedness (upper part) and left-handedness (lower part) when the electric field was varied between 1.09 and 1.32 V/μm. The positive and negative emission intensities denote the laser emission with right-handedness and left-handedness of circular polarization, respectively. (**C**) R-CP and L-CP laser emission intensity as a function of the polarization angle in the polar coordinate system from the heliconical superstructure in the PSS_{vis} state and PSS_{UV} state, respectively, where the polar angle ω stands for the transmission angle of the polarizer and the radius r stands for the transmittance.

The periodic hierarchical architecture of a well-arranged helicoidal superstructure revealed a typical photonic band gap (PBG) effect, which resembles a one-dimensional (1D) photonic crystal and has been confirmed to be a high efficient resonator for mirrorless tunable lasing after loading the gain medium into the system. Achieving a laser emission that has both a broad tunable spectral range and a switchable polarization by external stimulation, without any complicated structure, materials, or optical design, is desired by scientists and engineers. This laser could furnish extensive applications including increasing integration and minimizing the size of photonic devices or chips, as well as promoting the accuracy and precision of spectral analysis. So far, wavelength of laser tuned in a wide spectral range around more than 100 nm enabled by photoresponsive helicoidal LC helix functionalized with azobenzene-based molecular switch has been intensively reported (*27*–*29*); however, the prominent problem for practical application is the inevitable thermal relaxation of the molecular switch. On another aspect, electrically tunable laser based on a common helicoidal LC helix indicated that the emission wavelength was tuned in a narrow spectral range of tens of nanometers. A wide range of at least 100 nm modulated by electric field was lastly achieved using a heliconical LC helix recently; however, the polarization state of the emission was immutable, although its spectral tunable range was satisfied (*30*). Here, a dynamic and reversible tunable laser emission under the manipulation of a dual-stimulation strategy is demonstrated. The emission wavelength can be shifted within a relatively wide spectral range around 120 nm; moreover, the polarization state can be switched reversibly between the right-handed circular polarization (R-CP) and the left-handed circular polarization (L-CP). Such a dual-parameter tunability is enabled mainly by the specifically designed cholesteric LC system by adding a small amount (0.5 wt %) of the fluorescent dye, 4-(dicyanomethylene)-2-tert-butyl-6-(1,1,7,7-tetramethyljulolidin-4-yl-vinyl)-4H-pyran (DCJ; Tokyo Chemical Industry), as the gain medium (see fig. S9). As aforementioned, the original right-handedness helicoidal helix was reconfigured to the heliconical one as a 0.67 V/μm electric field was applied (Fig. 2A, ii); however, the laser emission was not detected as the sample was excited by a 532-nm focused pulsed laser, even the output energy of pump laser was higher enough (Fig. 3A) on account of nonoverlapping between the fluorescent spectrum of the gain medium and PBG of the corresponding heliconical superstructure. An R-CP laser emission with a wavelength of 710 nm as the electric field was enhanced to 1.09 V/μm was then detected and continuously blueshifted to 590 nm by gradually raising the electric field to 1.32 V/μm (Fig. 3B). Further increase in electric field caused the disappearance of the emission due to the same reason mentioned above. This R-CP emission can be switched to L-CP readily by stimulating the right-handedness system to a left-handedness one using UV irradiation, while the wavelength can be tuned within almost the same spectral range from 713 to 593 nm (Fig. 3B). The polarization state of each laser emission was corroborated by converting the circular polarization to a linear polarization using a quarter wave plate (QWP), i.e., an R-CP and an L-CP emission were converted to a linear polarized light along the direction of 135° and 45°, respectively (section S6). This linear polarized direction can be distinguished by recording the transmittance of the light after passing through a followed rotated analyzer (Fig. 3C). Desirable laser performances, including a narrow

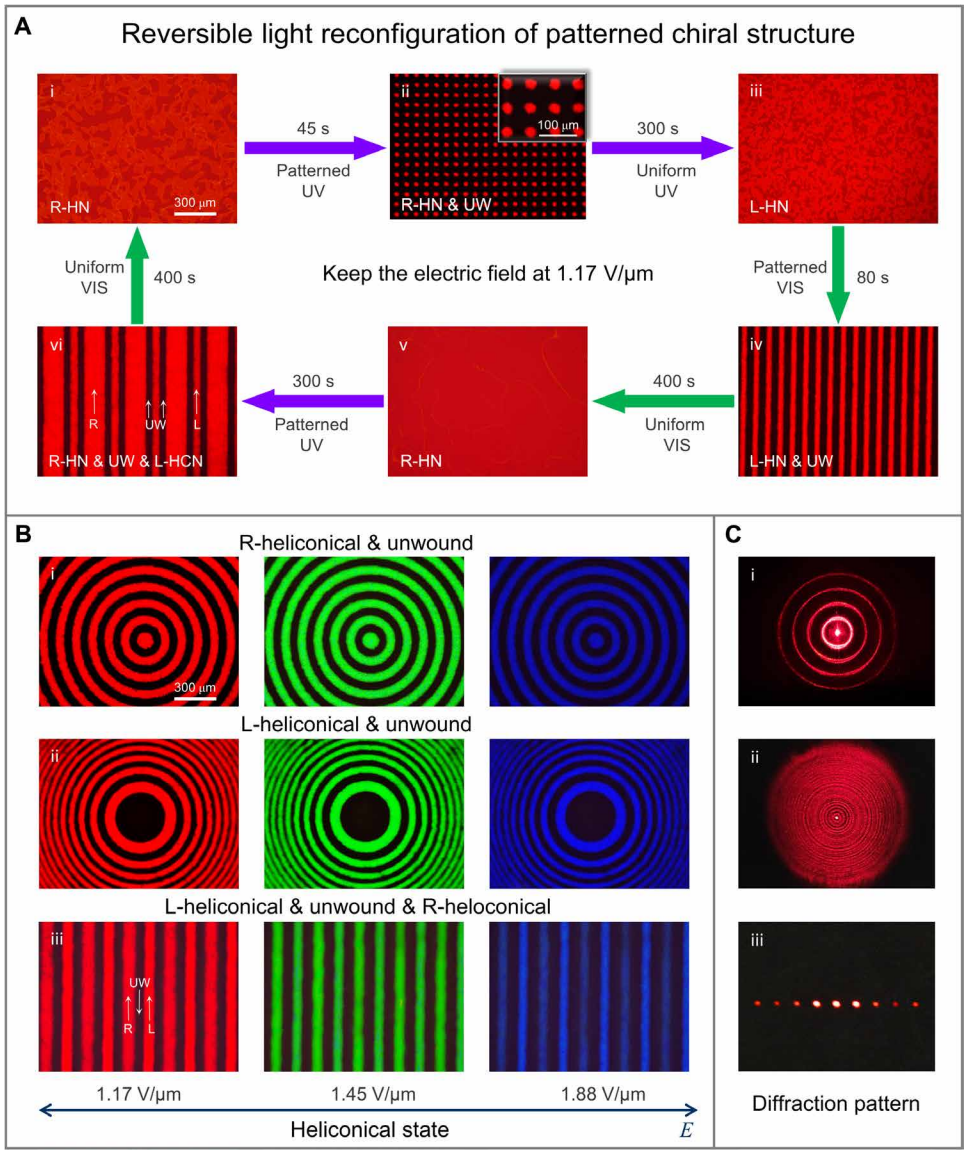

Fig. 4. Electric tunable micropatterns with prescribed microregions of molecular architectures by photopatterning. (**A**) Reversible photopatterning and photoerasing. (i) The PSS_{vis} state of the uniform heliconical texture exhibiting homogeneous red reflection at an electric field of 1.17 V/μm. (ii) Dosage-controlled UV irradiation (1.8 mW/cm^2) through a photomask results in a two-dimensional (2D) circular pattern composed of periodic distribution of nematic and right-handedness heliconical regions. The inset shows the local enlarged micrograph of the 2D pattern. In exposed regions, the twist toque is reduced as a result of the decrease in the effective chirality, leading to the homeotropic state under the electric field. One may refer to the phototuning dynamics in Fig. 2C. (iii) Uniform abundant UV irradiation erased the afore-recorded pattern into the homogeneous left-handedness heliconical superstructure showing red reflection. (iv) Dosage-controlled visible irradiation (5.5 mW/cm^2) through a photomask results in a stripe pattern composed of periodic distribution of nematic and left-handedness heliconical regions. (v) Uniform abundant visible irradiation erases the afore-recorded pattern and transforms it into the homogeneous right-handedness heliconical superstructure. (vi) Abundant UV irradiation through a photomask results in 1D line grating composed of periodic left- and right-handedness heliconical regions. Uniform abundant visible irradiation erases the afore-recorded pattern into the homogeneous right-handedness heliconical superstructure state. The electric field is maintained as 1.17 V/μm throughout the whole process. (**B**) Reflection textures at different applied electric fields for (i) the concentric circles composed of regions of the nematic phase and the right-handedness heliconical superstructure, (ii) the Fresnel lens composed of regions of the nematic phase and the left-handedness heliconical superstructure, and (iii) the 1D line grating composed of regions of the right-handedness heliconical superstructure, the left-handedness heliconical superstructure, and the boundary nematic phase. (**C**) Diffraction patterns for (i) the circular grating, (ii) the Fresnel lens, and (iii) the 1D line grating at an electric field of 1.17 V/μm measured with an He-Ne laser beam at 632.8 nm. HN, heliconical state; UW, unwound state.

emission bandwidth (~0.8 nm) and a low pumping threshold (fig. S10), were maintained throughout the whole controlling process, featuring the high cavity quality of the dynamic helical superstructure. The results reveal that any laser emission, whatever the wavelength or the polarization state, can be accurately programmed and directed at will by a proper dual-stimulation strategy disclosed here, which paves a way to the multidimensional laser encoding and future encryption.

The coexistence of a chiral soft material with an achiral one or two chiral systems with an opposite handedness is an inscrutable,

interesting, but challenging scientific issue in thermodynamics and phase transition. A coexistence of a cholesteric phase and a nematic phase, showing a periodic square pattern formed by alternate cholesteric and nematic regions, has been obtained in a polymer-stabilized LC system (*31*); however, the pattern cannot be removed once it is formed owing to the polymer stabilization used to maintain the cholesteric arrangement of LC molecules. Here, the patterned biphase [Fig. 4, A (ii and iv) and B (i and ii)] containing heliconical the cholesteric phase and the nematic phase was generated through dual stimulation of electric field and light. Not merely limited on biphase coexistence, a more complicated patterned triphase [Fig. 4, A (vi) and B (iii)] had been attained as well in the same manner, presenting right-handedness heliconical cholesteric, nematic, and left-handedness heliconical cholesteric phase distributed successively. The mixing bounding area shows the dark nematic phase as a result of chirality counterbalance between regions of opposite handednesses (*32*). It is worth noting that the patterned biphase and triphase systems are photorewritable, i.e., the original formed pattern can be removed and rewritten to a prescribed pattern solely by alternate irradiation of UV and visible light only if an appropriate electric field was applied on the sample (Fig. 4A). Besides, the heliconical arrangement featured electric field–controlled reflection color from red to blue at the cholesteric phase region, thereby achieving a dynamic manipulated and reconfigured phase coexistence of whatever double or triple phases with a photorewritable well-defined micropattern (Fig. 4B). Light diffraction patterns (Fig. 4C), corresponding to the concentric circles (Fig. 4B, i), Fresnel featured concentric circles (Fig. 4B, ii), and periodic stripes (Fig. 4B, iii), were detected due to the refractive index modulation between the heliconical cholesteric phase and the electric field–induced homeotropic alignment of nematic phase, further confirming the generated micropatterns and manifesting the potential application on dynamic photonics (section S8). Furthermore, this photolocalized patterning also exhibits a possible application in other nonphotonic fields, for instance, chiral screening, which is always used in fine chemical engineering, biomedical engineering, and pharmaceutical engineering.

CONCLUSIONS

Helical superstructure is ubiquitous in nature, reflecting some of the inner connections of microscopic interactions. Leveraging a stable, dynamic, and multiparameter manipulation of a helix on demand opens a brilliant era for responsive materials and will promote a thriving development on relevant fields in the near future. The reversible transformation of helical LC arrangement, among the common helicoidal helix, the special heliconical helix, and their counterparts with inverse handedness, was proposed and achieved in a predesigned specific photoresponsive cholesteric LC system by the dual stimulation of electric field and light. Such a formidable attribute was available from a delicate equilibrium between the bend and twist elastic effects of the LC system, as well as an appropriate coupling among the rate of photoisomerization (i.e., light intensity), the dielectric torque (i.e., strength of electric field), and the elastic effect (i.e., the composition of LC system). To corroborate the performances in arrangement transformation, tunable laser emission with both a relatively wide spectral dynamic range and a switching between R-CP and L-CP emission was enabled in virtue of the manipulations on helical pitch length and handedness of heliconical arrangement after doped with the gain medium. Moreover, the fantastic coexistence of the LC phase, including the biphase system (i.e., cholesteric heliconical arrangement and unwound nematic arrangement) and the triphase (i.e., right-handedness cholesteric heliconical arrangement, electric field–induced homeotropic nematic arrangement, and left-handedness cholesteric heliconical arrangement) with a prescribed micropattern, was created and confirmed through the diffraction technique. Stimulus-directed diverse transformation in LC relevant self-organized soft helical superstructure provides some unique horizons and new insights to more concretely understand the relationship between the nanoscale molecular interactions and the microscale self-organized behaviors and thereby promotes further applications in photonics, chemistry, pharmacy, biological engineering, etc. In addition, the proposed phenomenon also predicts some linkages between the condensed matter physics and solid geometry.

MATERIALS AND METHODS

Materials

The LC mixture contains 52.6 wt % commercial eutectic nematic LC (E7, Slichem Co. Ltd., China), 43.4 wt % achiral bent-shaped LC dimer (CB7CB, synthesized in the laboratory), 0.5 wt % chiral dopant (R811, Merck, Germany), 3.0 wt % photoresponsive chiral molecular switch [(*s,s*)-BTTC, synthesized in the laboratory], and 0.5 wt.% laser dye DCJ (Tokyo Chemical Industry, Japan; fig. S9) for lasing generation. The chemical structure of the LC dimer CB7CB is formed by two rod-like cyanobiphenyl moieties directly linked by a flexible alkyl chain as shown in fig. S6, leading to a sufficiently small K_3. E7 and LC dimer CB7CB, the host of cholesteric LC, are both of positive dielectric anisotropies so that the LC director prefers to align parallel to the electric field. Then, the mixture was homogeneously mixed in a vial with the addition of a few drops of dichloromethane at 45°C. After evaporation of the solvent, the mixture [with a phase change in the following sequence: the isotropic phase (75°C), the cholesteric phase (18°C), and the homochiral N_{tb} phase] was loaded into LC cells by capillary action at 100°C and then slowly cooled to room temperature (i.e., 25°C optimized in experiment; see fig. S8) at a rate of 0.5°C/min and further stored in the dark for about 3 hours. LC cells were prepared by using indium tin oxide glass plates, which were spin coated with polyimide to generate homogeneous alignment. The cell gap was maintained by 35-μm Mylar spacers to obtain better laser performance.

Characterization

The electric field–manipulated helix transformation was studied by applying a 3-kHz alternating current square wave generated from a signal generator (AFG3022, Tektronix) passing through a signal amplifier (A600, FLC Electronics) across the samples. The reversible change of HTP and handedness inversion in LC mixture were implemented by means of being irradiated by a 530-nm collimated LED light source (M530L3, Thorlabs) and a mercury lamp (SunSpot 2, Uvitron) whose output light was collimated by a group of lenses and fixed with a 310-nm bandpass spectral filter (SF). The output intensity of the UV light and the visible light were adjusted to 1.8 and 5.5 mW cm^{-2}, respectively. POM textures were observed by a polarized optical microscope (LVPOL 100, Nikon) and recorded by a charge-coupled device camera (DS-U3, Nikon) with two crossed linear polarizers in the reflection mode. A fiber-coupled spectrometer (Avaspec-ULS2048, resolution: ~2.0 nm, 200 to 1100 nm) was used to detect the reflection spectra from the sample under the illumination of a white light source

(Balanced deuterium-halogen light source, AvaLight-DHc). The polarization state of reflected light was determined by converting the CP light to linear polarization through a QWP, followed by detecting the polarization direction with a rotated analyzer. For photopatterning, the exciting light, either from a UV light source (SunSpot 2, Uvitron) or a visible source (M530L3, Thorlabs), after being expanded and precisely collimated by a group of lenses, illuminated the sample through a chromium photomask (SVG Optronics Co. Ltd.), which is in close contact with the prepared cell. The transmitted patterned light directs the formation of different superstructures in prescribed regions. Diffractive properties of the sample with light-patterned superstructures are characterized by a He-Ne laser.

Lasing emission

Lasing performance was analyzed using a 532-nm linearly polarized second harmonic Q-switched neodymium-doped yttrium aluminum garnet (Nd: YAG) pulsed laser (Dawa 200, Beamtech) with a repetition rate of 10 Hz and a pulse duration of 8 ns. First, the pump beam was focused by a spherical lens. Then, a slit was placed at the focus of the lens to filter the stray light and ensure the intensity uniformity of the pumping beam, followed by an expanding and refocusing on the sample by another spherical lens to a ~50-μm waist at an oblique incidence of ~45° to the cell substrate normal. A set of neural density filters (NDFs) was inserted to adjust the pump energy. A beam splitter was placed between the NDFs and sample for a real-time detection of pump energy by a pyroelectric energy sensor (ES111C, Thorlabs). Laser emission was detected by a high-resolution fiber-coupled spectrometer (Avaspec-ULS2048CL-EVO, resolution: ~0.3 nm, 360 to 860 nm). A longpass SF (cutoff wavelength, <550 nm) was placed between the sample and the fiber detector to eliminate the effect of the stray pump beam. A QWP at the wavelength of 632 nm and a polarizer were used to determine polarization properties.

SUPPLEMENTARY MATERIALS

Supplementary material for this article is available at http://advances.sciencemag.org/cgi/content/full/5/10/eaax9501/DC1

Fig. S1. Schematic illustration of LC director configurations in helicoidal, heliconical, and unwound superstructures as a function of the electric field.
Fig. S2. Electrical tuning performance of the heliconical superstructure.
Fig. S3. Simulated selective reflection spectra in the right-handed heliconical superstructure with various applied electric fields in the cases of R-CP incidence and L-CP incidence.
Fig. S4. Theoretical investigation of the effects of the photoinduced chirality changes on switching performance.
Fig. S5. Calculated reflection spectra from the heliconical superstructure as a function of the electric field and light stimuli.
Fig. S6. Chemical structure of the LC dimer CB7CB.
Fig. S7. Optimization of the cholesteric LC material system.
Fig. S8. UV-visible changes of (*s,s*)-BTTC in tetrahydrofuran solution and the thermal stability and fatigue resistance of closed-ring isomers.
Fig. S9. Characterization of the optical properties of the laser dye DCJ.
Fig. S10. Emission intensity as a function of pump energy for the right-handed heliconical resonator and the left-handed heliconical resonator.
References (*33*–*39*)

REFERENCES AND NOTES

1. M.-M. Giraud-Guillea, L. Besseau, R. Martin, Liquid crystalline assemblies of collagen in bone and in vitro systems. *J. Biomech.* **36**, 1571–1579 (2003).
2. V. Sharma, M. Crne, J. O. Park, M. Srinivasarao, Structural origin of circularly polarized iridescence in jeweled beetles. *Science* **325**, 449–451 (2009).
3. S. Vignolini, P. J. Rudall, A. V. Rowland, A. Reed, E. Moyroud, R. B. Faden, J. J. Baumberg, B. J. Glover, U. Steiner, Pointillist structural color in *Pollia* fruit. *Proc. Natl. Acad. Sci. U.S.A.* **109**, 15712–15715 (2012).
4. S. Vignolini, T. Gregory, M. Kolle, A. Lethbridge, E. Moyroud, U. Steiner, B. J. Glover, P. Vukusic, P. J. Rudall, Structural colour from helicoidal cell-wall architecture in fruits of *Margaritaria nobilis*. *J. R. Soc. Interface* **13**, 20160645 (2016).
5. D. Zerrouki, J. Baudry, D. Pine, P. Chaikin, J. Bibette, Chiral colloidal clusters. *Nature* **455**, 380–382 (2008).
6. G. Singh, H. Chan, A. Baskin, E. Gelman, N. Repnin, P. Král, R. Klajn, Self-assembly of magnetite nanocubes into helical superstructures. *Science* **345**, 1149–1153 (2014).
7. Y. Yin, Y. Xia, Self-assembly of spherical colloids into helical chains with well-controlled handedness. *J. Am. Chem. Soc.* **125**, 2048–2049 (2003).
8. W.-J. Chung, J.-W. Oh, K. Kwak, B. Y. Lee, J. Meyer, E. Wang, A. Hexemer, S.-W. Lee, Biomimetic self-templating supramolecular structures. *Nature* **478**, 364–368 (2011).
9. C. Mao, W. Sun, Z. Shen, N. C. Seeman, A nanomechanical device based on the B–Z transition of DNA. *Nature* **397**, 144–146 (1999).
10. J. Bath, A. J. Turberfield, DNA nanomachines. *Nature Nanotech.* **2**, 275–284 (2007).
11. M. Kumar, P. Brocorens, C. Tonnelé, D. Beljonne, M. Surin, S. J. George, A dynamic supramolecular polymer with stimuli-responsive handedness for in situ probing of enzymatic ATP hydrolysis. *Nature Commun.* **5**, 5793 (2014).
12. H. K. Bisoyi, A. M. Urbas, Q. Li, Soft materials driven by photothermal effect and their applications. *Adv. Optical Mater.* **6**, 1800458 (2018).
13. H. K. Bisoyi, T. J. Bunning, Q. Li, Stimuli-driven control of the helical axis of self-organized soft helical superstructures. *Adv. Mater.* **30**, 1706512 (2018).
14. S. Tokunaga, Y. Itoh, H. Tanaka, F. Araoka, T. Aida, Redox-responsive chiral dopant for quick electrochemical color modulation of cholesteric liquid crystal. *J. Am. Chem. Soc.* **140**, 10946–10949 (2018).
15. M. E. McConney, V. P. Tondiglia, L. V. Natarajan, K. M. Lee, T. J. White, T. J. Bunning, Electrically induced color changes in polymer-stabilized cholesteric liquid crystals. *Adv. Optical Mater.* **1**, 417–421 (2013).
16. Y.-C. Hsiao, K.-C. Huang, W. Lee, Photo-switchable chiral liquid crystal with optical tristability enabled by a photoresponsive azo-chiral dopant. *Opt. Express* **25**, 2687–2693 (2017).
17. P. Mach, R. Pindak, A.-M. Levelut, P. Barois, H. T. Nguyen, H. Baltes, M. Hird, K. Toyne, A. Seed, J. W. Goodby, C. C. Huang, L. Furenlid, Structures of chiral smectic-C mesophases revealed by polarization-analyzed resonant x-ray scattering. *Phys. Rev. E* **60**, 6793–6802 (1999).
18. J. P. Abberley, R. Killah, R. Walker, J. M. D. Storey, C. T. Imrie, M. Salamończyk, C. Zhu, E. Gorecka, D. Pociecha, Heliconical smectic phases formed by achiral molecules. *Nature Commun.* **9**, 228 (2018).
19. D. Chen, J. H. Porada, J. B. Hooper, A. Klittnick, Y. Shen, M. R. Tuchband, E. Korblova, D. Bedrov, D. M. Walba, M. A. Glaser, J. E. Maclennan, N. A. Clark, Chiral heliconical ground state of nanoscale pitch in a nematic liquid crystal of achiral molecular dimers. *Proc. Natl. Acad. Sci. U.S.A.* **110**, 15931–15936 (2013).
20. J. Xiang, Y. Li, Q. Li, D. A. Paterson, J. M. D. Storey, C. T. Imrie, O. D. Lavrentovich, Electrically tunable selective reflection of light from ultraviolet to visible and infrared by heliconical cholesterics. *Adv. Mater.* **27**, 3014–3018 (2015).
21. D. A. Paterson, J. Xiang, G. Singh, R. Walker, D. M. Agra-Kooijman, A. Martínez-Felipe, M. Gao, J. M. D. Storey, S. Kumar, O. D. Lavrentovich, C. T. Imrie, Reversible isothermal twist–bend nematic–nematic phase transition driven by the photoisomerization of an azobenzene-based nonsymmetric liquid crystal dime. *J. Am. Chem. Soc.* **138**, 5283–5289 (2016).
22. Y. Li, C. Xue, M. Wang, A. Urbas, Q. Li, Photodynamic chiral molecular switches with thermal stability: From reflection wavelength tuning to handedness inversion of self-organized helical superstructures. *Angew. Chem. Int. Ed. Engl.* **52**, 13703–13707 (2013).
23. D. W. Berreman, Optics in stratified and anisotropic media: 4 × 4-matrix formulation. *J. Opt. Soc. Am.* **62**, 502–510 (1972).
24. J. S. Patel, R. B. Meyer, Flexoelectric electro-optics of a cholesteric liquid crystal. *Phys. Rev. Lett.* **58**, 1538–1540 (1987).
25. A. Dewar, P. J. Camp, Dipolar interactions, molecular flexibility, and flexoelectricity in bent-core liquid crystals. *J. Chem. Phys.* **123**, 174907 (2005).
26. A. Mukherjee, M. Rahman, S. S. Bhattacharyya, B. K. Chaudhuri, A. Yoshizawa, High dielectric behavior and memory effect in a deformed helix ferroelectric liquid crystal with an antiferroelectric phase. *Chem. Phys. Lett.* **443**, 71–75 (2007).
27. Z.-g. Zheng, B.-w. Liu, L. Zhou, W. Wang, W. Hu, D. Shen, Wide tunable lasing in photoresponsive chiral liquid crystal emulsion. *J. Mater. Chem. C* **3**, 2462–2470 (2015).
28. T.-H. Lin, Y.-J. Chen, C.-H. Wu, A. Y.-G. Fuh, J.-H. Liu, P.-C. Yang, Cholesteric liquid crystal laser with wide tuning capability. *Appl. Phys. Lett.* **86**, 161120 (2005).
29. G. Petriashvili, M. A. Matranga, M. P. D. Santo, G. Chilaya, R. Barberi, Wide band gap materials as a new tuning strategy for dye doped cholesteric liquid crystals laser. *Opt. Express* **17**, 4553–4558 (2009).
30. J. Xiang, A. Varanytsiaa, F. Minkowski, D. A. Paterson, J. M. D. Storey, C. T. Imrie, O. D. Lavrentovich, P. Palffy-Muhoray, Electrically tunable laser based on oblique heliconical cholesteric liquid crystal. *Proc. Natl. Acad. Sci. U.S.A.* **113**, 12925–12928 (2016).

31. S. S. Choi, S. M. Morris, W. T. S. Huck, H. J. Coles, Simultaneous red-green-blue reflection and wavelength tuning from an achiral liquid crystal and a polymer template. *Adv. Mater.* **22**, 53–56 (2010).
32. G. W. Gray, D. G. McDonnell, The relationship between helical twist sense, absolute configuration and molecular structure for non-sterol cholesteric liquid crystals. *Mol. Cryst. Liq. Cryst.* **34**, 211–217 (1976).
33. R. B. Meyer, Effects of electric and magnetic fields on the structure of cholesteric liquid crystals. *Appl. Phys. Lett.* **12**, 281–282 (1968).
34. P. G. De Gennes, Calcul de la distorsion d'une structure cholesterique par un champ magnetique. *Solid State Commun.* **6**, 163–165 (1968).
35. D. K. Yang, S. T. Wu, *Fundamentals of Liquid Crystal Devices* (John Wiley and Sons, New Jersey, 2014).
36. H. Wöhler, G. Haas, M. Fritsch, D. Mlynski, Faster 4× 4 matrix method for uniaxial inhomogeneous media. *J. Opt. Soc. Am. A* **5**, 1554–1557 (1988).
37. V. Borshch, Y.-K. Kim, J. Xiang, M. Gao, A. Jákli, V. P. Panov, J. K. Vij, C. T. Imrie, M. G. Tamba, G. H. Mehl, O. D. Lavrentovich, Nematic twist-bend phase with nanoscale modulation of molecular orientation. *Nat. Commun.* **4**, 2635 (2013).
38. J. Xiang, S. V. Shiyanovskii, C. T. Imrie, O. D. Lavrentovich, Electrooptic response of chiral nematic liquid crystals with oblique helicoidal director. *Phys. Rev. Lett.* **112**, 217801 (2014).
39. S. M. Salili, J. Xiang, H. Wang, Q. Li, D. A. Paterson, J. M. D. Storey, C. T. Imrie, O. D. Lavrentovich, S. N. Sprunt, J. T. Gleeson, A. Jákli, Magnetically tunable selective reflection of light by heliconical cholesterics. *Phys. Rev. E* **94**, 042705 (2016).

Acknowledgments

Funding: We acknowledge support from the National Key Research and Development Program of China (2017YFA0303700), the National Science Foundation of China (grant nos. 61822504, 61575063, 61435008, and 51873060), the Shanghai Rising Star Program (grant no. 17QA1401100), the State Key Laboratory of Applied Optics (no. M200-D-1716), and the Ohio Third Frontier. **Author contributions:** Z.-g.Z., Y.Lu, and Q.L. designed the research. C.-l.Y., W.H., Z.-g.Z., and B.L. carried out the experiments. Y.Li synthesized the chiral molecular switch. C.-l.Y., W.H., Z.-g.Z., and H.K.B. prepared the manuscript. C.-l.Y., W.H., Z.-g.Z., B.L., H.K.B., Y.Li, D.S., Y.Lu, and Q.L. interpreted the results and contributed to the editing of this work. **Competing interests:** The authors declare that they have no competing interests. **Data and materials availability:** All data needed to evaluate the conclusions in the paper are present in the paper and/or the Supplementary Materials. Additional data related to this paper may be requested from the authors.

Submitted 7 May 2019
Accepted 9 September 2019
Published 4 October 2019
10.1126/sciadv.aax9501

Citation: C.-l. Yuan, W. Huang, Z.-g. Zheng, B. Liu, H. K. Bisoyi, Y. Li, D. Shen, Y. Lu, Q. Li, Stimulated transformation of soft helix among helicoidal, heliconical, and their inverse helices. *Sci. Adv.* **5**, eaax9501 (2019).